Available online at www.sciencedirect.com
ScienceDirect
Comput. Methods Appl. Mech. Engrg. 335 (2018) 52–68
Computer methods in applied mechanics and engineering
www.elsevier.com/locate/cma

# Modelling of strain softening materials based on equivalent damage force

Rade Vignjevic[a,*], Nenad Djordjevic[a], Tom De Vuyst[a], Simone Gemkow[b]

[a] *Dynamic Response Group, Structural Integrity Theme, Brunel University London, Kingston Lane Uxbridge, UB8 3PH, United Kingdom*
[b] *Cranfield University, Cranfield, Bedfordshire MK43 0AL, United Kingdom*

Received 29 October 2017; received in revised form 20 January 2018; accepted 28 January 2018
Available online 26 February 2018

**Abstract**

The main aim of the work presented in this paper was treatment of damage and deformation localisation observed in the finite element method (FEM) analysis of strain softening materials combined with local constitutive models where damage is represented using continuum damage mechanics (CDM). The CDM/FEM approach typically suffers from a number of shortcomings, including mathematical (change of the type of partial differential equations leading to ill-posed boundary value problem), numerical (pronounced mesh dependency) and physical (infinitely small softening zone with the zero dissipated energy). The approach proposed here is still based on the local constitutive model including damage, but introduces an alternative representation of damage effects in the system of linear momentum balance equations. The damage effects are included through equivalent damage force (EDF), which contributes to the right-hand side of the momentum balance equations. The main advantages of this approach are that the problem remains well posed, as the type of partial differential equations remains unchanged when the material enters softening; numerical stability is preserved without a need for regularisation measures; and significantly reduced mesh dependency. In addition, the EDF approach can be used in combination with existing local CDM damage models and does not violate symmetry of the material stiffness tensor.

The EDF approach is applicable to modelling of strain softening typically observed in damaged quasi brittle materials such as fibre reinforced composites and concrete.

The EDF model was implemented in the in-house developed coupled FEM-SPH code, where an explicit FEM code is coupled with a stable Total-Lagrange form of SPH. Its performance is demonstrated in the analysis of a dynamic one dimensional (1D) stress wave propagation problem, which was analytically solved by Bazant and Belytschko in 1985. For a range of loading rates that correspond to the material softening regime, the numerical results shown nonlocal character with a finite size of the damaged zone, controlled with the damage characteristic length, which can be experimentally determined and is an input parameter independent of the discretisation density.



*Keywords:* Strain softening instability; Damage localisation; FEM; Composite materials; Quasi brittle materials

* Corresponding author.
*E-mail address:* v.rade@brunel.ac.uk (R. Vignjevic).

https://doi.org/10.1016/j.cma.2018.01.049

## 1. Introduction

Strain softening is deterioration of material strength with increasing strain, which is a phenomenon typically observed at a continuum level in damaged quasi brittle materials, including fibre reinforced composites and concrete. It is primarily a consequence of brittleness and heterogeneity of the material. It has been experimentally demonstrated that the strain softening in the material is distributed over a finite region whose size depends on material type, see for instance [1] and references therein. Averaging is an approach to modelling the strain softening where micromechanical damage effects are smeared over the softening zone in Continuum Damage Mechanics (CDM). An example of damage model, that is often used in with the averaging, is the model where degradation of material properties is represented as a loss of effective load-carrying area [2–4].

When local CDM constitutive models are used with the finite element method (FEM), the strain softening leads to numerical instability, as the tangent stiffness tensor (slope of the stress–strain curve in 1D) loses positive definiteness and violates the material stability criterion by Hadamard [5]. Consequently, the underlying initial boundary value problem becomes ill-posed and the continuum solution bifurcates, leading to an infinite number of solutions. In addition, these local CDM models lead to deformation localised in a single element and consequently pronounced sensitivity of the results to the spatial discretisation (mesh density) as already demonstrated in [6]. Localised deformation and mesh sensitivity lead to infinite local strain with mesh refinement (in the limit). This result is non-physical with unrealistic energy dissipation due to damage within a zero volume zone. In summary, strain softening leads to mathematical pathology, in terms of change of the type of partial differential equations (PDE), numerical pathology, in terms of mesh sensitivity, and leads to the physically meaningless results.

The strain-softening instabilities have been of large interest to research in recent decades and have been investigated, among many others in [7–15], leading to a development of a number of regularisation methods, including non-local, gradient-enhanced and viscous methods. These methods are based on the introduction of a characteristic length scale into constitutive equations through higher-order spatial derivatives or viscous effects, see for instance the models developed by Dillon [16], Bazant [17,18], Aifantis [19,20], Needleman [21–23], Pijaudier-Cabot [24,7], Sluys [25,26], and de Borst [27–29]. These regularisation methods prevent development of the material instability i.e. prevent change of the type of underlying governing equations, which are elliptic partial differential equations in static problems and hyperbolic in dynamic problems. This in turn leads to a well-posed initial boundary value problem. The material characteristic length scale defines the size of the area affected by strain-softening enabling physically meaningful and mesh-independent finite element solutions.

Despite the evident success of regularisation methods in the field of strain-softening instabilities, research has been almost exclusively focused on these methods and, to date, there has been little research into solutions based on local constitutive equations. However, this might be of interest to users of strain-softening models as regularisation methods necessitate an increased understanding of the underlying strain-softening problem, definition of the characteristic length for the material of interest and make the application of regularisation methods numerically more expensive. More importantly, a suitable description of damage effects in a continuum combined with CDM, allows for more flexibility in formulation of constitutive models and related material experimental characterisation. We, among a number of other researchers, demonstrated that strain-softening results in numerical instability and highly mesh sensitivity in FEM analyses [6]. The aim of the work presented in this paper was development of an alternative new approach to modelling damage in strain softening materials within the FEM framework and based on the local constitutive equations. The model developed is called equivalent damage force (EDF). The key feature of this approach is that the material damage effects are represented as a force on the right-hand side of the balance of linear momentum equation. The proposed EDF method maintains a well-posedness of initial boundary value problems and, therefore, does not require any regularisation measures within constitutive equations in modelling strain-softening materials. In addition, the method can be combined with any CDM local damage law, providing the mesh independent stable solutions.

This paper consists of five sections. Following the introduction of the strain softening problem and associated issues, a benchmark dynamic strain softening problem is described in Section 2 with the analytical local and nonlocal solutions proposed by Bazant and Belytschko [30]. The Equivalent Damage Force approach is presented in Section 3, including the derivation of principle equations and model implementation into the in-house coupled FEM–SPH code. The proposed approach is validated against the known analytical solutions in Section 4, with the outcomes of this work summarised in Section 5.

## 2. Dynamic strain softening problem

### 2.1. Analytical solution

Development of localised deformation is a result of the physical damage processes occurring in the material at microscale, including initiation, growth and interaction of cracks and voids, which finally lead to complete material failure. In this investigation, a definition of localisation proposed in [31] is used: "Localization is defined as instability in the macroscopic constitutive description of inelastic deformation of the material".

Damage evolution in local constitutive law for a homogeneous material leads to a bifurcation point, where the material becomes unstable and the deformation localises within an infinitely small instability zone and becomes non-uniform. Outside this instability zone the material remains stable [31].

Material is stable and stays in equilibrium when the double contraction of true stress rate $\dot{\sigma}_{ij}$ and strain rate $\dot{\varepsilon}_{ij}$, given in (2.1) is positive. This criterion is also called general bifurcation criterion [8], and is satisfied as long as the material behaviour is determined with a positive definite stiffness tensor.

$$\dot{\varepsilon}_{ij}\dot{\sigma}_{ij} > 0. \tag{2.1}$$

The rate form of constitutive equations used here ensures a piecewise linear relationship between stress-rate and strain-rate, which can be expressed as a constitutive equation defined in terms of material tangent stiffness tensor $\mathbb{C}_{ijkl}$:

$$\dot{\sigma}_{ij} = \mathbb{C}_{ijkl}\dot{\varepsilon}_{kl}. \tag{2.2}$$

So that the inequality (2.1) reads:

$$\dot{\varepsilon}_{ij}\mathbb{C}_{ijkl}\dot{\varepsilon}_{kl} > 0. \tag{2.3}$$

The material becomes unstable when it reaches its bifurcation point i.e. when the condition in (2.3) is violated. Hence, the bifurcation point is defined as:

$$\dot{\varepsilon}_{ij}\mathbb{C}_{ijkl}\dot{\varepsilon}_{kl} = 0. \tag{2.4}$$

Condition (2.4) is satisfied when the tangent stiffness tensor becomes singular, i.e. $\mathbb{C}_{ijkl}$ is not positive-definite anymore, which corresponds to zero stiffness tensor determinant:

$$\det\left(\mathbb{C}_{ijkl}\right) = 0. \tag{2.5}$$

The initial analytical and later numerical investigation of strain-softening was carried out by analysing longitudinal wave propagation in a bar shown in Fig. 1. This problem, in context of local strain-softening continua, was first considered and analytically solved in [30] and has been repeatedly used by researchers working on strain-softening within the CDM framework and the investigation of regularisation methods, see for instance [17,26,28,32]. The problem concerns one-dimensional (1D) symmetrical stress wave propagation in a bar, which simplifies interpretation of the strain-softening effects and provides clarity. The bar, $2L$ long, is symmetrically loaded in tension at both ends with constant velocity $v$. In the original paper [30], the bar material behaviour is defined by stress–strain relationship illustrated in Fig. 1b, where the material softening (stress–strain curve segment between Point P and Point F) is characterised with a negative slope and elastic unloading/reloading law.

The symmetric loading of the bar generates two tensile step waves, which propagate towards the middle section of the bar ($x = 0$), where they are superposed at time $t = L/c$. Superposition of the waves in the middle section of the bar instantaneously doubles the strain. Depending on the magnitude of the superposed stress waves, softening of the material may be initiated. The time and condition for strain-softening initiation is determined using 1D wave equation as outlined below.

Complete derivation of the 1D wave equation (2.6) can be found in a number of textbooks (see for instance [32] or [33], pp. 1–33), valid for elastic and inelastic material behaviour, which is in its standard hyperbolic form for elastic behaviour given as:

$$\frac{\partial^2 u\,(x,t)}{\partial t^2} = \frac{1}{\rho}\frac{\partial \sigma}{\partial \varepsilon}\frac{\partial \varepsilon}{\partial x} = \frac{1}{\rho}\frac{\partial \sigma}{\partial \varepsilon}\frac{\partial^2 u\,(x,t)}{\partial x^2}, \qquad \frac{\partial^2 u\,(x,t)}{\partial t^2} = c^2\frac{\partial^2 u\,(x,t)}{\partial x^2} \tag{2.6}$$

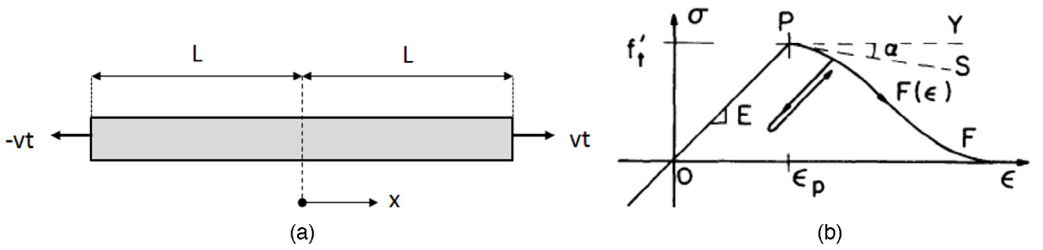


**Fig. 1.** (a) Geometry and loading of softening bar; (b) stress–strain behaviour [30].

where: $c$ is elastic speed of sound, $u\,(x,t)$ longitudinal displacement, $x$ is longitudinal coordinate and $t$ is time. Please note that the elastic speed of sound of isotropic material, for the uniaxial stress and uniaxial strain state propagation problem are respectively defined as:

$$c = \sqrt{\frac{E}{\rho}} \tag{2.7}$$

$$c = \sqrt{\frac{E\,(1-\nu)}{\rho\,(1-2\nu)\,(1+\nu)}} \tag{2.8}$$

with $E$ and $\nu$ being Young's modulus and Poisson's ratio. Analytical solution for this stress wave propagation problem can be derived starting from for the longitudinal displacement function used in analysis of elastic longitudinal wave propagation in a semi-infinite bar proposed in [34] as:

$$u\,(x,t) = -v\left\langle t - \frac{x+L}{c}\right\rangle + v\left\langle t + \frac{x-L}{c}\right\rangle \tag{2.9}$$

where the brackets $\langle\cdot\rangle$ represent positive definite expressions and $L$ is half of the bar length. The corresponding strain $\varepsilon_x$ and stress $\sigma_x$ components in the loading direction are defined as [6]:

$$\varepsilon_x = \frac{\partial u}{\partial x} = \frac{v}{c}\left[H\left(t - \frac{x+L}{c}\right) + H\left(t + \frac{x-L}{c}\right)\right] \tag{2.10}$$

$$\sigma_x = \frac{E\,(1-\nu)}{(1-2\nu)\,(1+\nu)}\varepsilon_x \tag{2.11}$$

where $H$ is Heaviside function.

Superposition of the waves in the middle section of the bar ($x = 0$) at response time $t = L/c$ instantaneously doubles the strain $\varepsilon_x = v/c$. The loading conditions, i.e. particle velocity $v(x)$ at $x = -L$ and $x = L$ control the loading strain magnitude $\varepsilon_L = \varepsilon(x = -L) = \varepsilon(x = L)$ depending on which one can distinguish the following three possible scenarios:

(1) the loading strain satisfies condition $\varepsilon_L \leq \varepsilon_p/2$, the bar is elastically deformed during the whole loading process, and assumption of linear elasticity holds even after the waves superposition, i.e. until both waves travel the whole bar length;
(2) the loading strain satisfies condition $\varepsilon_p/2 \leq \varepsilon_L \leq \varepsilon_p$, the bar is elastically loaded for the time $0 \leq t < L/c$; however, at $t = L/c$, material instantaneously enters the strain-softening regime for which the solution for the longitudinal displacement given by Eq. (2.9) holds only for the elastic part of the response, i.e. $t < L/c$;
(3) the loading strain satisfies condition $\varepsilon_L > \varepsilon_p$, the bar undergoes inelastic deformation from the beginning of the loading $t = 0$, which is not considered in this paper;

Please note that $\varepsilon_p$, which is elastic limit for the material, needs to be defined for both the uniaxial stress and uniaxial strain states, where the latter is given in Eq. (2.10).

In the work presented in this paper, the second scenario given above is considered, where following the superposition of the tensile waves at $t = L/c$, the slope of the stress–strain curve in Fig. 1, becomes negative, i.e. $F'(\varepsilon) = \frac{\partial \sigma}{\partial \varepsilon} < 0$, and wave speed becomes imaginary so that the equation of motion in the softening domain becomes an elliptic PDE:

$$c^2 \frac{\partial^2 u(x,t)}{\partial x^2} + \frac{\partial^2 u(x,t)}{\partial t^2} = 0 \text{ where } c^2 = \frac{F'(\varepsilon)}{\rho} \text{ and } \rho = \rho_0 \frac{1}{1+\varepsilon_{ii}}. \tag{2.12}$$

Because of the material softening, a discontinuity in displacement develops at $x = 0$, with the difference in magnitude equal to $4v\langle t - L/c\rangle$, and strain increases infinitely with the stress dropping to zero, whilst the rest of the bar starts to unload elastically. The infinite strain in the softening domain can be expressed using the Dirac Delta function $\delta(x)$ as:

$$\varepsilon_x = 4v\langle t - L/c\rangle \delta(x) \tag{2.13}$$

with the strain field outside the softening zone, for $t > L/c$ and $x < 0$, defined as:

$$\varepsilon_x = \frac{v}{c}\left[H\left(t - \frac{x+L}{c}\right) - H\left(t + \frac{x-L}{c}\right) + 4v\langle t - L/c\rangle \delta(x)\right] \tag{2.14}$$

The solution (2.14) is symmetric with respect to $x = 0$.

Using the equations above, analytical solutions for displacement, strain stress and internal energy in the strain softening problem, at the response time $t = 3L/2c$, are shown in Fig. 2. The key difference between the elastic solution and the strain softening (local) solution is that elastic solution provides continuous wave propagation after superposition, whereas local solution features the discontinuity in the displacements and development of the standing strain wave in the middle section of the bar. The obtained discontinuity could not propagate away from the localisation zone, due to the change of nature of the PDEs in this zone from hyperbolic to elliptic. Consequently, material unloads outside of the localisation zone and the softening zone acts as a free boundary.

The results shown in Fig. 2 are compared with numerical results of the newly developed EDF model in Section 4.

## 3. Equivalent damage force model

Our first attempt to model the strain softening problem illustrated in Fig. 1, using both SPH and FEM, was published in [6]. In a series of numerical experiments, it was shown that the size or width of the strain softening region was controlled by the element size in classic FEM, with the strain softening localised in a single layer of elements. In SPH, the size of the softening zone was controlled by the smoothing length, rather than the inter-particle distance, which demonstrates that the SPH method is inherently non-local and suggests that the SPH smoothing length should be linked to the material characteristic length scale in solid mechanics simulations.

To address the localisation problem observed in the FEM combined with the classic CDM, an alternative approach to modelling damage localisation is proposed here. Instead of using tangential stiffness to represent stiffness of damaged material, which leads to imaginary wave speed in softening material, damage is incorporated in a form of equivalent damage force (EDF). This force is added to resultant force acting at a point in the solid, i.e. the right-hand side of the linear momentum balance PDE so that the homogeneous part of the PDE remains unchanged relative to the elastic solution. This allows for PDEs to maintain their hyperbolic character and boundary value problem to remain well posed. The primary objective of the proposed approach is to avoid the damage induced strain softening instabilities characterised with imaginary speed of sound. Derivation of EDF is given below for an isotropic softening material.

### 3.1. Derivation of the equivalent damage force

Derivation of the EDF starts with the definition of the effective stress $\overline{\sigma}$ [2,4], which is given in Eq. (3.15), and calculation of the stress divergence used in the balance of linear momentum (3.17) as:

$$\overline{\sigma} = \frac{\sigma}{1-\omega} \tag{3.15}$$

$$\nabla \cdot \sigma = \nabla \cdot \overline{\sigma} - \nabla \cdot (\omega \overline{\sigma}) = \nabla \cdot \overline{\sigma} - (\nabla \cdot \omega)\overline{\sigma} - \omega(\nabla \cdot \overline{\sigma}) \tag{3.16}$$

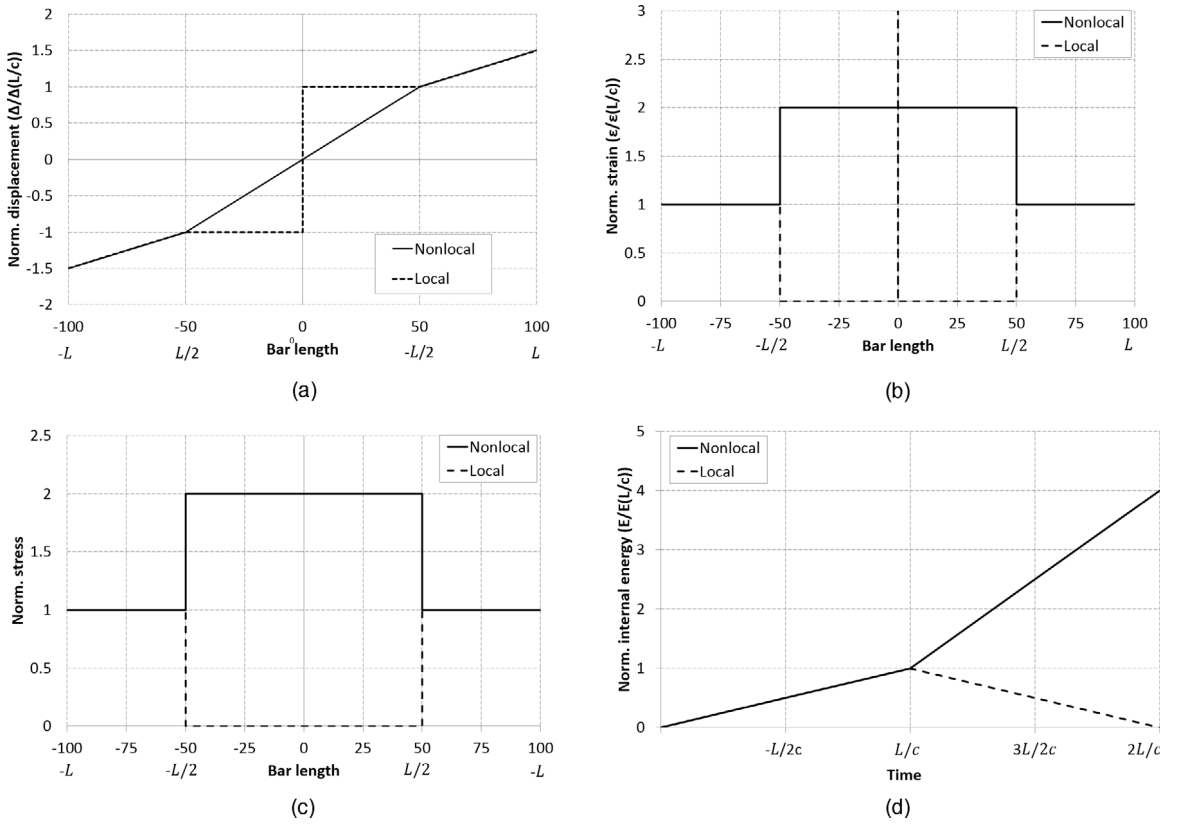


**Fig. 2.** Elastic local and nonlocal solutions at response time $t = 3L/2c$ for: (a) normalised displacement; (b) normalised strain; (c) normalised stress; (d) normalised internal energy.

$$\nabla \cdot \sigma + b = \rho a \tag{3.17}$$

Where: $\sigma$ is true stress, $\omega$ is damage variable, $b$ is a body force vector, $\rho$ is material density and $a$ is acceleration vector. A weak form of the conservation law (3.17) can now be written in the Voigt notation as:

$$\begin{aligned}&\int_\Omega \rho\{\delta w\}^T\{\ddot{u}\}\,dV + \int_\Omega \{\nabla\cdot\delta w\}^T\{\overline{\sigma}\}\,dV - \int_\Omega \{\delta w\}^T\{\nabla\cdot\omega\}\{\overline{\sigma}\}\,dV - \\ &\int_\Omega \{\delta w\}^T\{\omega\}\{\nabla\cdot\overline{\sigma}\}\,dV - \int_\Omega \{\delta w\}^T\{b\}\,dV - \int_\Gamma \left(\{\delta w\}^T\{\overline{\sigma}\}\right)\cdot n d\Gamma = 0\end{aligned} \tag{3.18}$$

$$\begin{aligned}&\{\delta d\}^T\left[\int_\Omega \rho[N]^T[N]\left\{\ddot{d}\right\}dV + \int_\Omega [B]^T\{\overline{\sigma}\}\,dV - \int_\Omega [N]^T\{\nabla\cdot\omega\}\{\overline{\sigma}\}\,dV - \right. \\ &\left.\int_\Omega [N]^T\{\omega\}\{\nabla\cdot\overline{\sigma}\}\,dV - \int_\Omega [N]^T\{b\}\,dV - \int_\Gamma \left([N]^T\{\overline{\sigma}\}\right)\cdot n d\Gamma\right] = 0\end{aligned} \tag{3.19}$$

$$\begin{aligned}&\int_\Omega \rho[N]^T[N]\left\{\ddot{d}\right\}dV + \int_\Omega [B]^T\{\overline{\sigma}\}\,dV - \int_\Omega [N]^T\{\nabla\cdot\omega\}\{\overline{\sigma}\}\,dV - \\ &\int_\Omega [N]^T\{\omega\}\{\nabla\cdot\overline{\sigma}\}\,dV - \int_\Omega [N]^T\{b\}\,dV - \int_\Gamma \left([N]^T\{\overline{\sigma}\}\right)\cdot n d\Gamma = 0\end{aligned} \tag{3.20}$$

where a standard FEM notation for matrix of shape functions $[N]$ and strain displacement matrix $[B]$ was used in the expressions above, together with test function (virtual displacement vector) denoted as $\{\delta w\}$. Differential equation of

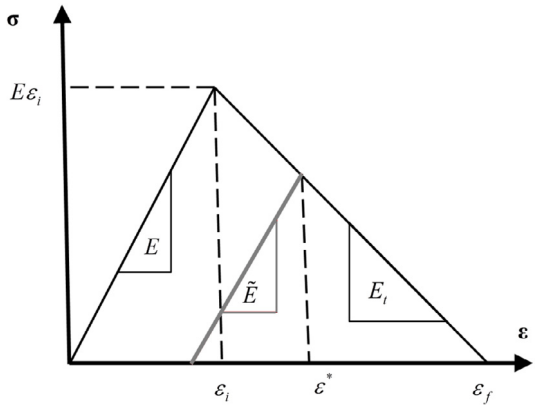


**Fig. 3.** Bilinear law implemented in the classical FEM and EDF codes using a damage parameter $\omega$ and CDM approach.

motion (3.20) can be rewritten as:

$$[M]\left\{\ddot{d}\right\} + [K]\{d\} = \{f\}_D + \{f\}_b + \{f\}_e \tag{3.21}$$

where the following definitions are used:

$$\begin{aligned}
[M] &= \int_\Omega \rho [N]^T [N] \left\{\ddot{d}\right\} dV && \text{— mass matrix} \\
[K] &= \int_\Omega [B]^T \mathbb{C} [B]\, dV && \text{— stiffness matrix} \\
\{f\}_D &= \int_\Omega [N]^T \{\nabla\omega\} \{\overline{\sigma}\}\, dV + \int_\Omega [N]^T \{\omega\} \{\nabla \cdot \overline{\sigma}\}\, dV && \text{— equivalent damage force} \\
\{f\}_b &= \int_\Omega [N]^T \{b\}\, dV && \text{— body force vector} \\
\{f\}_e &= \int_\Gamma \left([N]^T \{\overline{\sigma}\}\right) \cdot n d\Gamma && \text{— traction on a boundary.}
\end{aligned} \tag{3.22}$$

In this derivation, damage contributes to the momentum balance through the term $\{f\}_D$ in Eq. (3.21), which requires at least one of the integrals calculated for a damaged element, to be nonzero.

### 3.2. EDF implementation

EDF was initially developed in combination with a scalar damage model for under-integrated linear solid elements. This implies constant strain and constant stress/effective stress within an element. Consequently, the second term in Eq. (3.22) is equal to zero, whilst the first term in the equation is determined by damage function used.

Given that the character of the analytical solution for strain softening problem is independent of the specific shape of the damage function, i.e. precise value $F'(\varepsilon) < 0$ of the stress–strain curve shown in Fig. 1, and the intent to apply the model to composite materials, EDF was implemented together with bilinear constitutive law shown in Fig. 3. Evolution of damage is defined in terms of a single damage variable $\omega$, using a local CDM. The material softening and the damage evolution can occur when strain is in the range between $\varepsilon_i$ and $\varepsilon_f$.

The damage and the tangent stiffness, i.e. slope of the stress–strain curve, for the material state determined by $\varepsilon^*$, were respectively calculated as:

$$\omega = 1 - \frac{\varepsilon_i \left(\varepsilon_f - \varepsilon^*\right)}{\varepsilon^* \left(\varepsilon_f - \varepsilon_i\right)} \tag{3.23}$$

$$E_T = -\frac{E\varepsilon_i}{\varepsilon_f - \varepsilon_i} \tag{3.24}$$

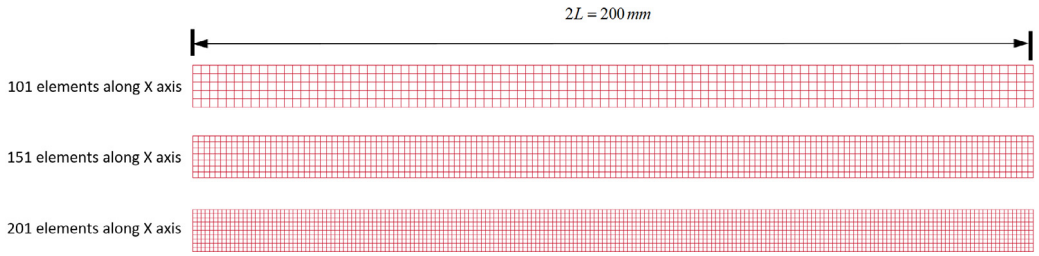


**Fig. 4.** Mesh densities used in the bar strain-softening problem.

**Table 1**
Mesh density used in the FEM models of strain softening problem.

| Number of elements | Impact direction $x$ | In-plane $y$ | In-plane $z$ |
|---|---|---|---|
| Mesh 1 | 101 | 5 | 5 |
| Mesh 2 | 151 | 7 | 7 |
| Mesh 3 | 201 | 10 | 10 |

In the equations above, $E$ is a Young modulus of undamaged material. Gradient of damage, i.e. derivative of damage parameter in the bilinear constitutive law with respect to coordinate $x$, can be calculated from Eq. (3.23), making use of a chain rule as:

$$\frac{\partial \omega}{\partial x} = \frac{\partial \omega}{\partial \varepsilon}\frac{\partial \varepsilon}{\partial x} \tag{3.25}$$

which is for linear elements equal to zero. This makes the first term in Eq. (3.22) and total equivalent damage force in a damaged linear solid element equal to zero. This problem can be overcome by using higher order element formulation, which provides nonzero gradient of damage and divergence of stress tensors. Alternatively, the damage gradient and divergence of stress tensors in Eq. (3.22) can be calculated numerically, which results in a nonzero EDF even for the under-integrated/linear elements. Consequently, the numerically calculated EDF is adopted in this work, as outlined below.

Divergence of stress and gradient of damage in the EDF model are calculated using the following generic approximation for gradient of function $f(x)$:

$$\nabla f(\boldsymbol{x}_I) = \sum_J \frac{m_J}{\rho_J} f(\boldsymbol{x}_J) \left[\nabla W\left(\left|\boldsymbol{x}_I - \boldsymbol{x}_J\right|, l_\omega\right)\right] \tag{3.26}$$

where indices $I$ and $J$ denote actual and neighbouring element integration points, respectively; $x_I$ and $x_J$ are integration point coordinates, $m_J$ and $\rho_J$ are mass and density of the neighbouring element, $W$ is weighting function and $l_\omega$ is material characteristic damage length, which is an input parameter for the EDF model. The EDF model was implemented in the Lawrence Livermore National Laboratory (LLNL) Non-Linear Transient Finite Element Code Dyna3d [35–38]. The numerical results obtained with the model are given in the following section.

## 4. Numerical experiments

The dynamic strain softening problem described in Section 2 was modelled here in a series of numerical experiments, which complement the work published in [6]. Although the strain-softening bar problem is symmetric, the bar was discretised with odd number of elements in the loading direction, with a layer of elements/integration points in the midsection of the bar, which did not allow for application of the symmetric boundary conditions. Constitutive model defined in Fig. 3 was used with three FEM solid element models shown in Fig. 4, with mesh densities defined in Table 1. The minimum mesh density, i.e. element size in the loading direction, was defined so that the wave propagation across an element occurs at least over three time steps, with the element aspect ratio equal to 1. The mesh density is also consistent with the discretisation used in the previously published SPH simulations.

The test programme consisted of three numerical experiments. In all three experiments the bar was symmetrically loaded in tension by applying constant velocity to the bar ends:

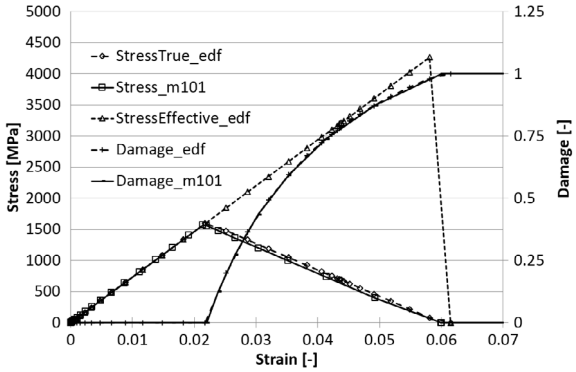


**Fig. 5.** Stress vs. strain and damage vs. strain relationships obtained with CDM and EDF models; mesh 1 model with 101 elements in the impact direction.

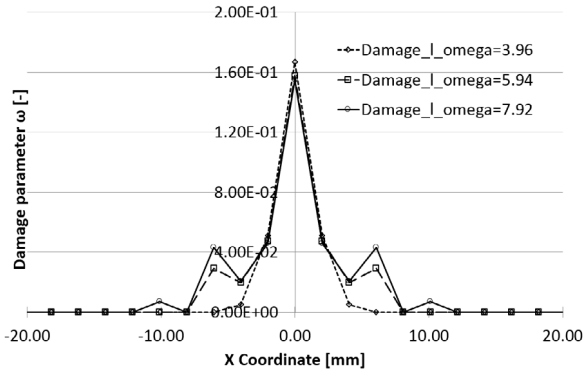


**Fig. 6.** Damage distribution in the middle of the bar in experiment 1 at response time $t = 3L/2$; three simulations performed with three damage characteristic lengths.

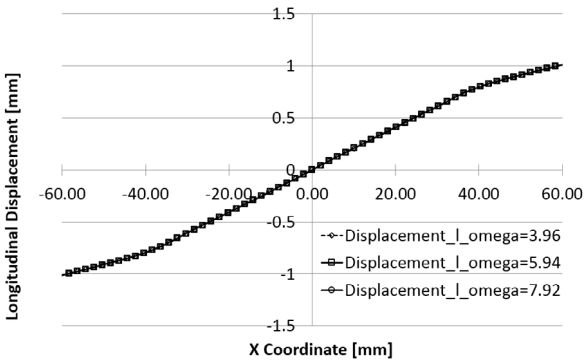


**Fig. 7.** Longitudinal displacement distribution in the middle of the bar in experiment 1 at response time $t = 3L/2$; three simulations performed with three damage characteristic lengths.

(1) Experiment 1 was performed with mesh 1 for a loading velocity $v = 70 \times 10^3$ mm/s, with three different damage characterisation lengths $l_\omega$ (material input parameter);
(2) Experiment 2 was performed with three mesh densities defined in Table 1 for a loading velocity $v = 70 \times 10^3$ mm/s, with the reference damage characteristic length $l_\omega$;
(3) Experiment 3 was performed with mesh 1 for a loading velocity $v = 80 \times 10^3$ mm/s, with the reference damage characteristic length $l_\omega$.

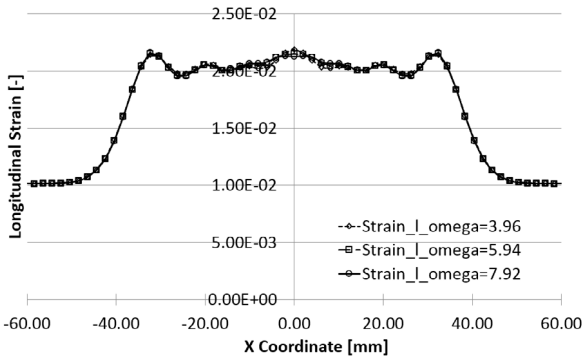


**Fig. 8.** Longitudinal strain distribution in the middle of the bar in experiment 1 at response time $t = 3L/2$; three simulations performed with three damage characteristic lengths.

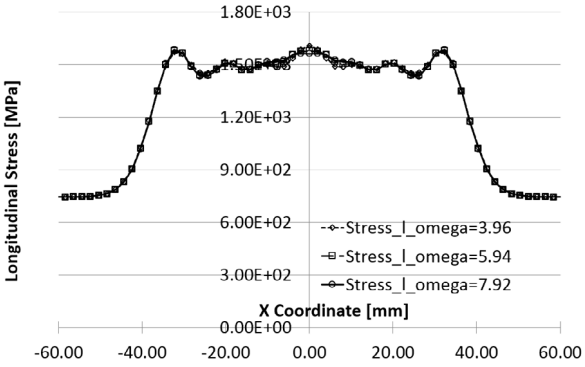


**Fig. 9.** Longitudinal stress distribution in the middle of the bar in experiment 1 at response time $t = 3L/2$; three simulations performed with three damage characteristic lengths.

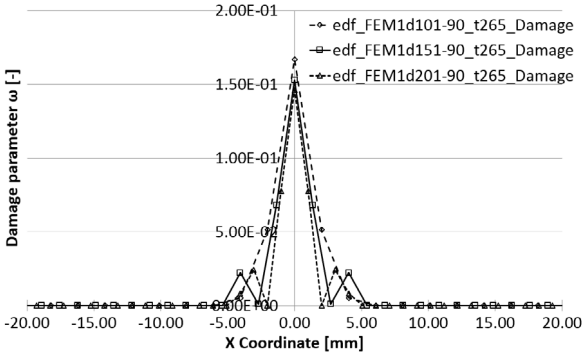


**Fig. 10.** Damage distribution in the middle of the bar in experiment 2 at response time $t = 3L/2$; three mesh densities performed with the same damage characteristic length.

The first two experiments are consistent with the numerical experiments published in [6] and correspond to the maximum strain developed in the midsection of the bar to be very close to the strain softening initiation (beginning of the softening behaviour), whilst the experiment 3 is chosen with the maximum strain very close to the total failure.

True stress–strain, effective stress–strain and damage–strain relationships, obtained in the impact direction with the classic CDM and the EDF approach, are given in Fig. 5. The curves were obtained with the FEM models with 101 elements along the impact direction (mesh 1) and use the same damage function defined in Eq. (3.23) as illustrated in

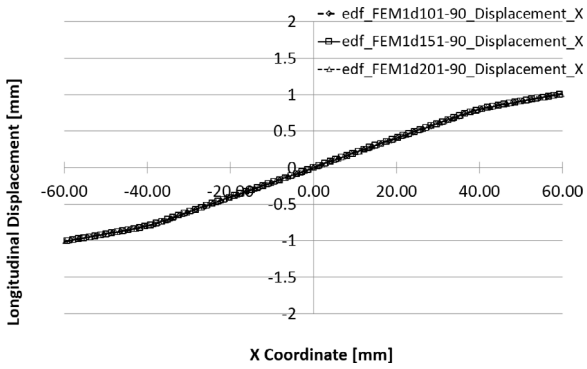


**Fig. 11.** Longitudinal displacement distribution in the middle of the bar in experiment 2 at response time $t = 3L/2$; three mesh densities performed with the same damage characteristic length.

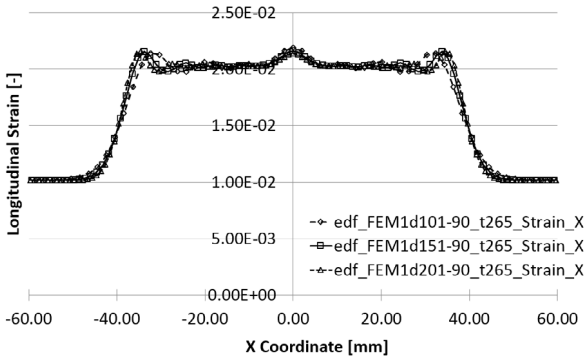


**Fig. 12.** Longitudinal strain distribution in the middle of the bar in experiment 2 at response time $t = 3L/2$; three mesh densities performed with the same damage characteristic length.

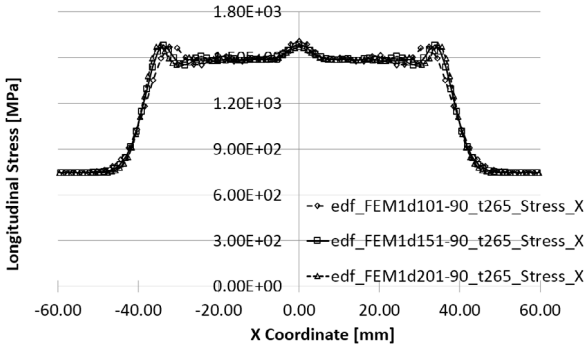


**Fig. 13.** Longitudinal stress distribution in the middle of the bar in experiment 2 at response time $t = 3L/2$; three mesh densities performed with the same damage characteristic length.

the figure. The slope of the effective stress–strain curve of the EDF model in presence of damage is equivalent to the slope of the elastic model. At the point of complete failure, which corresponds to $\omega = 1$, material stiffness in the EDF model drops to zero in a single step as the element is removed from the further calculation.

The simulation results of the experiment 1 for damage, displacement, strain and stress distribution, obtained at the response time $t = 3L/2$, when the stress wave propagated three quarters of the bar length, are respectively shown from Figs. 6 to 9. The simulations were run with the reference mesh 1 and three values for damage characteristic

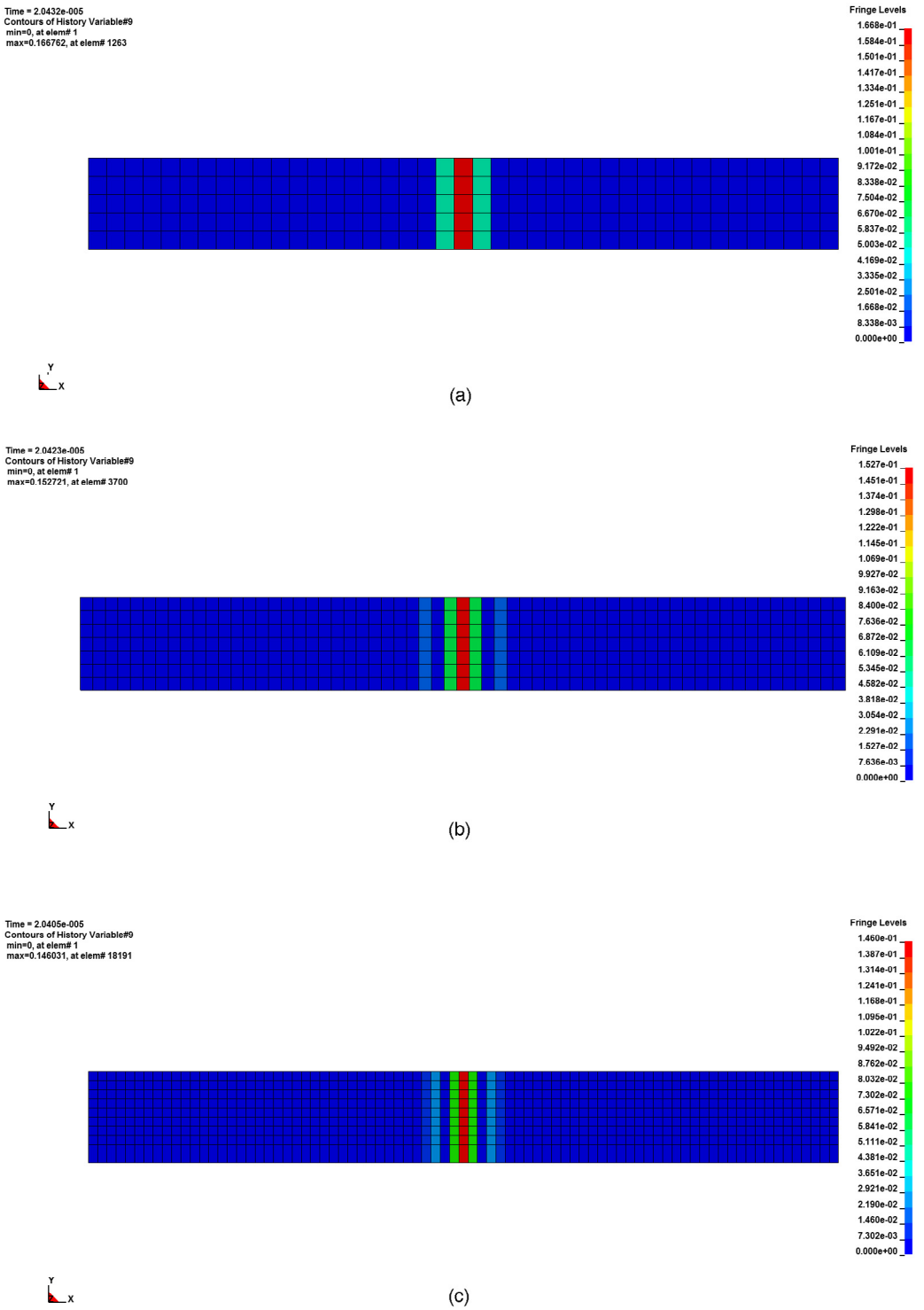


**Fig. 14.** Nonlocal damage distribution in the middle of the bar for three mesh densities with constant characteristic damage length: (a) mesh 1; (b) mesh 2; (c) mesh 3.

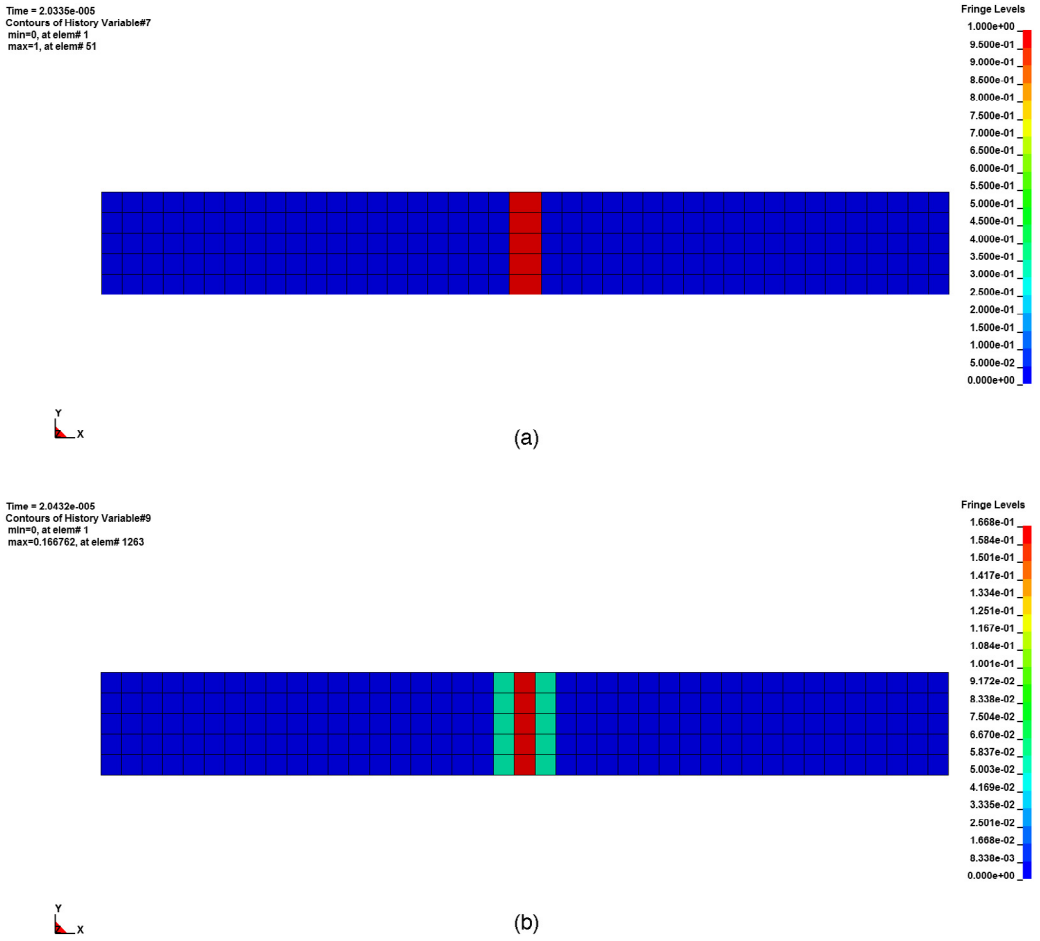


**Fig. 15.** Damage distribution in the middle of the bar for the model with 101 elements in the impact direction: (a) classic FEM; (b) EDF model.

lengths: $l_{\omega 1} = 3.96$ mm, $l_{\omega 2} = 5.94$ mm and $l_{\omega 1} = 7.92$ mm. The obtained results shown a pronounced nonlocal character, with the size of the damaged zone controlled by the damage characteristic length.

Consequently, experiment 2 was carried out with three mesh densities and reference damage characteristic length $l_{\omega} = 3.96$ mm (an input parameter for the EDF model). The results for the damage, displacement, strain and stress distribution are shown from Figs. 10 to 13. The results are stable and consistent with the nonlocal analytical solutions presented in Fig. 2, with damage distributed over a finite zone which is approximately $3l_{\omega}$ wide, as illustrated in Figs. 10–14. Damage distribution obtained in these simulations is independent of discretisation density unlike in the classic FEM results where damage is localised in a single layer of elements in the midsection of the bar as it can be seen from Figs. 15 to 17. The maximum value of damage parameter observed in the midsection of the bar in the EDF results was equal to $\omega = 0.1668$, rather than $\omega = 1.0$, which was the value obtained in the local classic FEM solution (see for instance Fig. 15).

The third experiment was performed for the impact velocity which induced almost complete failure in the midsection of the bar. The obtained results are still nonlocal and comparison of the distribution of the state variables with the results obtained in the second experiment is given in Figs. 18–21.

## 5. Summary

As already stated the SPH method is inherently non-local, with the smoothing length related to the material damage/failure characteristic length, and not sensitive to interparticle distance (no spatial discretisation/mesh

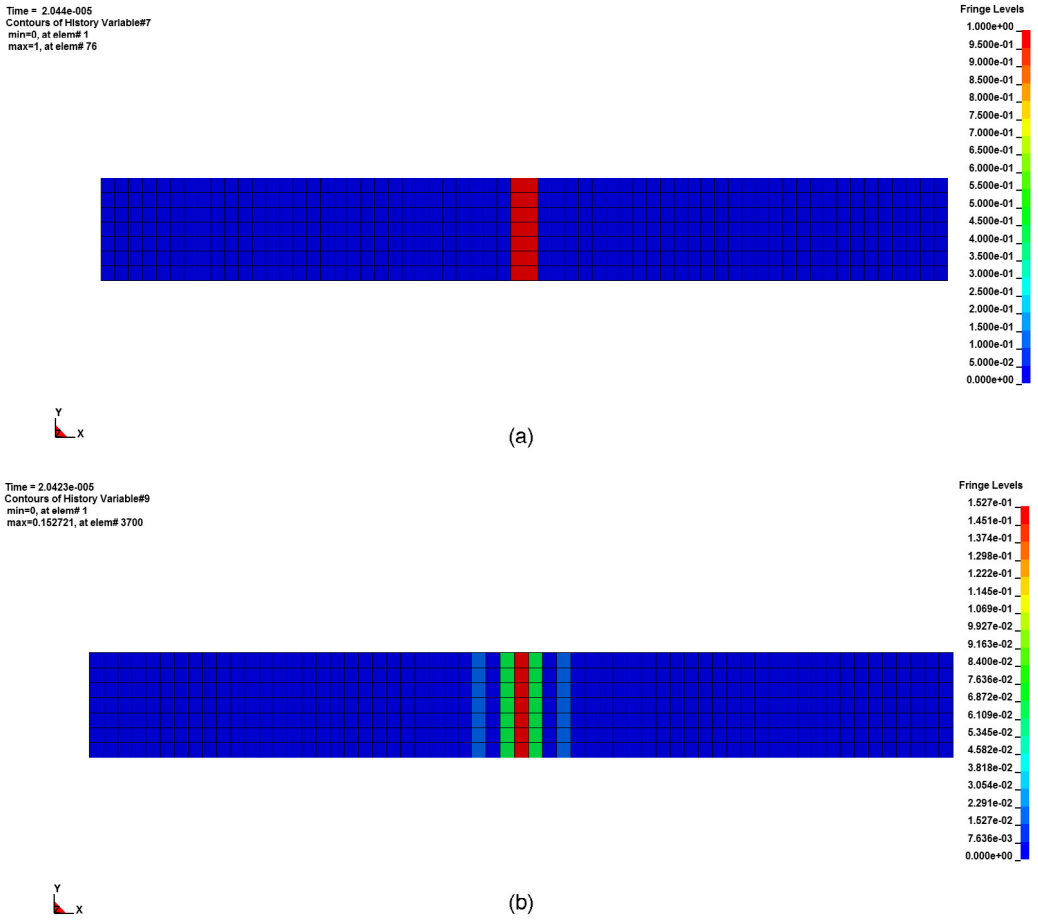


**Fig. 16.** Damage distribution in the middle of the bar for the model with 151 elements in the impact direction: (a) classic FEM; (b) EDF model.

sensitivity). This makes SPH better suited than conventional FEM for modelling of damage localisation in solid mechanics.

In the EDF approach material damage effects are represented as damage effect force which contributes to the right-hand side of the linear momentum balance equation. In the proposed form of the method, calculation of the damage force requires numerical determination of stress divergence and damage gradient. Size of the domain over which these derivatives are approximated determines the size of the softening zone (material damage characteristic length).

Presented numerical examples demonstrate that the EDF model effectively deals with the main shortcomings of classical FEM when used with local constitutive models in simulations of damage induced material softening, including mesh sensitivity (softening region size controlled by the element size) and non-physical localisation of deformation in single layer of elements.

For the test cases considered, the numerical results obtained with EDF show stable and nonlocal character, with a reduced mesh dependency, where the size of damaged zone was controlled with damage characteristic length (EDF model input parameter). Another important characteristic of the EDF model is that it can be combined with local constitutive models which include local CDM damage models.

The future work will include extension of the EDF model to 3D and anisotropic material models suitable for composite materials.

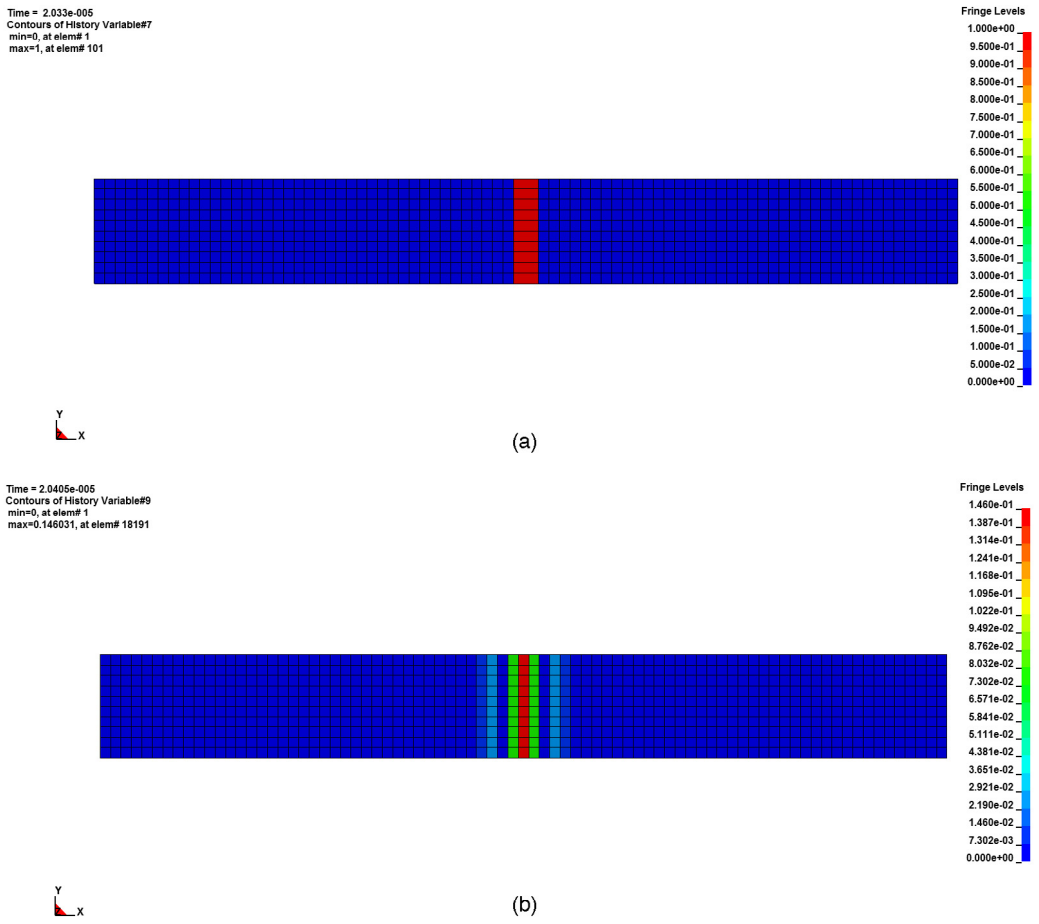


**Fig. 17.** Damage distribution in the middle for the bar model with 201 elements in the impact direction: (a) classic FEM; (b) EDF model.

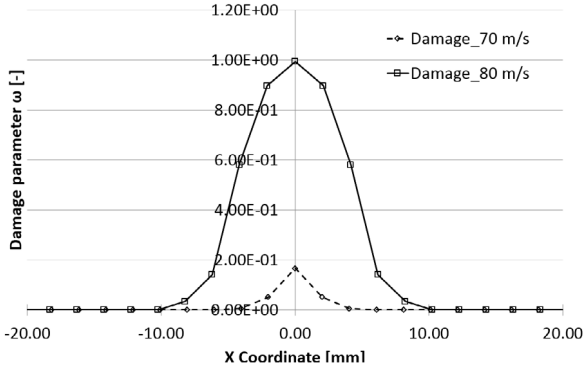


**Fig. 18.** Damage distribution in the middle of the bar for 101 element model for experiment 2 and experiment 3 at response time $t = 3L/2$.

## Acknowledgement

The project leading to this publication has received funding from the European Union's Horizon 2020 research and innovation programme under grant agreement No. 636549.

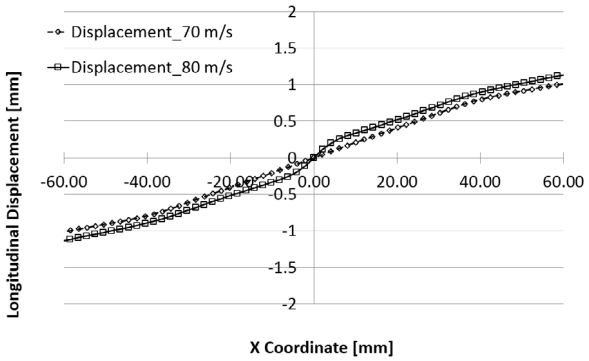


**Fig. 19.** Longitudinal displacement distribution in the middle of the bar for the 101 element model for experiment 2 and experiment 3 at response time $t = 3L/2$.

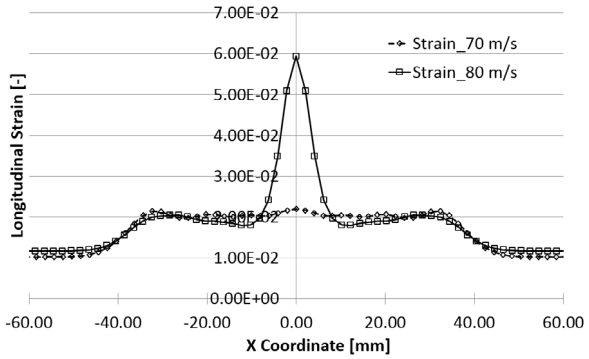


**Fig. 20.** Longitudinal strain distribution in the middle of the bar for the 101 element model for experiment 2 and experiment 3 at response time $t = 3L/2$.

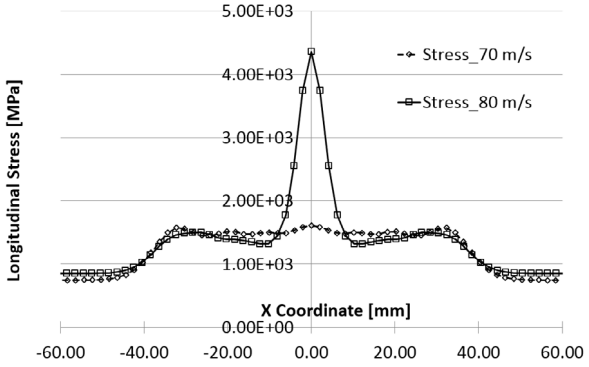


**Fig. 21.** Longitudinal stress distribution in the middle of the bar for the 101 element model for experiment 2 and experiment 3 at response time $t = 3L/2$.

## References

[1] Z.P. Bazant, T.B. Belytschko, T. Chang, Continuum theory for strain-softening, J. Eng. Mech. 110 (12) (1984) 1666–1692.
[2] L.M. Kachanov, Time of the rupture process under creep conditions, Izv. Akad. Nauk SSSR, Otd. Teckhn. Nauk 8 (1958) 26–31.
[3] J. Lemaitre, Coupled elasto-plasticity and damage constitutive equations, Comput. Methods Appl. Mech. Engrg. 51 (1–3) (1985) 31–49.
[4] D. Krajcinovic, Damage Mechanics, Elsevier, Amsterdam, New York, 1996.
[5] J.S. Hadamard, Cours du College de France. Leçons sur la propagation des ondes et les équations de l'hydrodynamique, Paris.

[6] R. Vignjevic, N. Djordjevic, S. Gemkow, T. De Vuyst, J. Campbell, SPH as a nonlocal regularisation method: Solution for instabilities due to strain-softening, Comput. Methods Appl. Mech. Engrg. 277 (2014) 281–304.
[7] G. Pijaudier-Cabot, Z.P. Bazant, M.R. Tabbara, Comparison of various models for strain softening, Eng. Comput. 5 (2) (1988) 141–150.
[8] M.K. Neilsen, H.L. Schreyer, Bifurcations in elastic–plastic materials, Int. J. Solids Struct. 30 (4) (1993) 521–544.
[9] L.J. Sluys, R. De Borst, Dispersive properties of gradient-dependent and rate-dependent media, Mech. Mater. 18 (2) (1994) 131–149.
[10] F. Armero, D. Ehrlich, An analysis of strain localization and wave propagation in plastic models of beams at failure, Comput. Methods Appl. Mech. Engrg. 193 (30–32) (2004) 3129–3171.
[11] R. Chambon, D. Caillerie, C. Tamagnini, A strain space gradient plasticity theory for finite strain, Comput. Methods Appl. Mech. Engrg. 193 (27–29) (2004) 2797–2826.
[12] F.R. Ahad, K. Enakoutsa, K.N. Solanki, D.J. Bammann, Nonlocal modelling in high-velocity impact failure of 6061-t6 aluminium, Int. J. Plast. 55 (2014) 108–132.
[13] G.D. Nguyen, A.M. Korsunsky, J.P. Belnoue, A nonlocal coupled damage-plasticity model for the analysis of ductile failure, 2015.
[14] C. Dascalu, Dynamic localization of damage and microstructural length influence, Int. J. Damage Mech. 26 (8) (2017) 1190–1218.
[15] T. Brepols, S. Wulfinghoff, S. Reese, Gradient-extended two-surface damage-plasticity: Micromorphic formulation and numerical aspects, Int. J. Plast. 97 (2017) 64–106.
[16] O.W. Dillon Jr., J. Kratochvil, A strain gradient theory of plasticity, Int. J. Solids Struct. 6 (12) (1970) 1513–1533.
[17] Z.P. Bazant, A. Zubelewicz, Strain-softening bar and beam: Exact non-local solution, Int. J. Solids Struct. 24 (7) (1988) 659–673.
[18] Z.P. Bazant, M. Jirasek, Nonlocal integral formulations of plasticity and damage: Survey of progress, J. Eng. Mech. 128 (11) (2002) 1119–1149.
[19] E.C. Aifantis, On the Microstructural Origin of Certain Inelastic Models, 1984.
[20] E.C. Aifantis, On the role of gradients in the localization of deformation and fracture, Internat. J. Engrg. Sci. 30 (10) (1992) 1279–1299.
[21] A. Needleman, Material rate dependence and mesh sensitivity in localization problems, Comput. Methods Appl. Mech. Engrg. 67 (1) (1988) 69–85.
[22] V. Tvergaard, A. Needleman, Effects of nonlocal damage in porous plastic solids, Int. J. Solids Struct. 32 (8–9) (1995) 1063–1077.
[23] V. Tvergaard, A. Needleman, Nonlocal effects on localization in a void-sheet, Int. J. Solids Struct. 34 (18) (1997) 2221–2238.
[24] G. Pijaudier-Cabot, Z.P. Bazant, Nonlocal damage theory, J. Eng. Mech. 113 (10) (1987) 1512–1533.
[25] L.J. Sluys, R. De Borst, Wave propagation and localization in a rate-dependent cracked medium-model formulation and one-dimensional examples, Int. J. Solids Struct. 29 (23) (1992) 2945–2958.
[26] L.J. Sluys, R. De Borst, Dispersive properties of gradient-dependent and rate-dependent media, Mech. Mater. 18 (2) (1994) 131–149.
[27] R.H.J. Peerlings, R. De Borst, W.A.M. Brekelmans, M.G.D. Geers, Wave propagation and localisation in nonlocal and gradient-enhanced damage models, J. Phys. IV 8 (8) (1998) Pr8–293–Pr8–300.
[28] R.H.J. Peerlings, M.G.D. Geers, R. De Borst, W.A.M. Brekelmans, A critical comparison of nonlocal and gradient-enhanced softening continua, Int. J. Solids Struct. 38 (44–45) (2001) 7723–7746.
[29] R.H.J. Peerlings, R. De Borst, W.A.M. Brekelmans, M.G.D. Geers, Localisation issues in local and nonlocal continuum approaches to fracture, Eur. J. Mech. A 21 (2) (2002) 175–189.
[30] Z.P. Bazant, T.B. Belytschko, Wave propagation in a strain-softening bar: Exact solution, J. Eng. Mech. 111 (3) (1985) 381–389.
[31] J.W. Rudnicki, J.R. Rice, Conditions for the localization of deformation in pressure-sensitive dilatant materials, J. Mech. Phys. Solids 23 (6) (1975) 371–394.
[32] K.F. Graff, Wave Motion in Elastic Solids, Dover, New York, 1991.
[33] W. Johnson, Impact Strength of Materials, Edvard Arnold Limited, 1972, pp. 1–33.
[34] T. Von Karman, P. Duwez, The propagation of plastic deformation in solids, J. Appl. Phys. 21 (10) (1950) 987–994.
[35] J. Liu, Dyna3D: A Nonlinear, Explicit, Three-Dimensional Finite Element Code for Solid and Structural Mechanics, University of California, Lawrence Livermore National Laboratory, Livermore, (CA) USA, 2004.
[36] R. Vignjevic, J.R. Reveles, J. Campbell, SPH in a total lagrangian formalism, CMES - Comput. Model. Eng. Sci. 14 (3) (2006) 181–198.
[37] R. Vignjevic, J. Campbell, J. Jaric, S. Powell, Derivation of SPH equations in a moving referential coordinate system, Comput. Methods Appl. Mech. Engrg. 198 (30–32) (2009) 2403–2411.
[38] T. De Vuyst, R. Vignjevic, Total lagrangian sph modelling of necking and fracture in electromagnetically driven rings, Int. J. Fract. 180 (1) (2013) 53–70.